Progress In Electromagnetics Research, PIER 77, 43–54, 2007

COMPACT ARTIFICIAL MAGNETIC CONDUCTOR DESIGNS USING PLANAR SQUARE SPIRAL GEOMETRIES

Y. Kim, F. Yang, and A. Z. Elsherbeni

Electrical Engineering Department
University of Mississippi
University, MS 38677, USA

Abstract—Compact spiral artificial magnetic conductors (AMC) have been investigated in this paper. First, single and double spirals are examined to achieve an in-phase reflection at a lower frequency compared to a conventional patch element of the same size. However, these two designs generate a large cross polarization. The cross polarization affects the operating frequency and bandwidth. In order to eliminate the cross polarization effect, a four-arm spiral element is introduced. This geometry does not generate a cross polarization, and an operating frequency that is 49.45% lower than the reference patch element has been achieved.

1. INTRODUCTION

Recent investigations for the design a low profile antenna relies on artificial material with specific electromagnetic properties. Among those are the man made metamaterial [1–4], band gap structures (EBG) [5–11], high impedance surfaces, [12, 13], and artificial magnetic conductors (AMC). Electromagnetic band-gap (EBG) structures are used to reduce printed antenna size and to reduce the mutual coupling in array configurations[10, 11]. When plane waves illuminate on an EBG surface, the reflection phase continuously changes from 180° to −180° with the increasing frequency. Especially at the 0° reflection phase in a certain frequency band, the surface shows the property of a perfect magnetic conductor (PMC). The PMC material does not exist in nature, but an artificial magnetic conductor (AMC) can be realized from the property of the EBG structure.

In this paper, a compact AMC design that minimizes the cross polarization effect of printed spiral geometry will be presented. There

have been proposed various AMC surfaces such as mushroom-like EBG structure [14], Hilbert-Curve [15], Jerusalem Crosses [16], dipole and slot arrays [17]. In particular, the Hilbert-Curve inclusion focuses on the compactness of the surface. As the number of iteration order increases, the equivalent inductance increases, resulting in a lower resonant frequency. With the similar idea to the Hilbert-Curve inclusion, a larger equivalent inductance can also be realized with a larger number of spiral turns. However, as revealed in this paper, if a unit geometry is not symmetric with respect to the polarizations of the incident waves, the AMC surface generates a high level of cross polarization. Thus, the behavior of reflection phase may not be applicable in the designated frequency band of operation due to the existence of cross polarization. Several typical printed spiral geometries are investigated in this paper and their reflection phase characteristics are reported.

2. SPIRAL AMC DESIGNS

2.1. Reference Geometry and Design Methods

For the purpose of comparison, the reflection phase characteristic of a conventional mushroom-like EBG structure [6] is introduced first. Figure 1a shows a unit cell of the EBG structure, where a square metal patch is placed on top of a grounded substrate and a conducting via connects the top metal patch and the ground plane. The thickness of the substrate is $0.04\,\lambda_{12GHz}$, the width of substrate is $0.15\,\lambda_{12\mathrm{GHz}}$, and the relative permittivity of the substrate is 2.2. The width of center metal patch is $0.13\,\lambda_{12\mathrm{GHz}}$ and the vias radius is assumed to be infinitely thin in the simulation. Periodic boundary conditions (PBC) are put on four sides of the unit cell to model the effect of periodic replication in an infinite array structure.

The finite-difference time-domain method (FDTD) [18] is used to analyze this configuration of the EBG structure. A normally incident plane wave is launched at a source plane, and the reflected fields are calculated at an observation plane, as shown in Fig. 1a. To retrieve the reflection phase on the top surface of the EBG structure, a PEC ground located at the same height is independently simulated as a reference. The reflection phase is then calculated using the following equation:

$$\theta = \theta^{\mathrm{EBG}} - \theta^{\mathrm{PEC}} + \pi \tag{1}$$

A radian of π is added because the PEC ground has a reflection phase of π [6]. To verify the computation results, the Ansoft Designer software is also used for the AMC analysis.

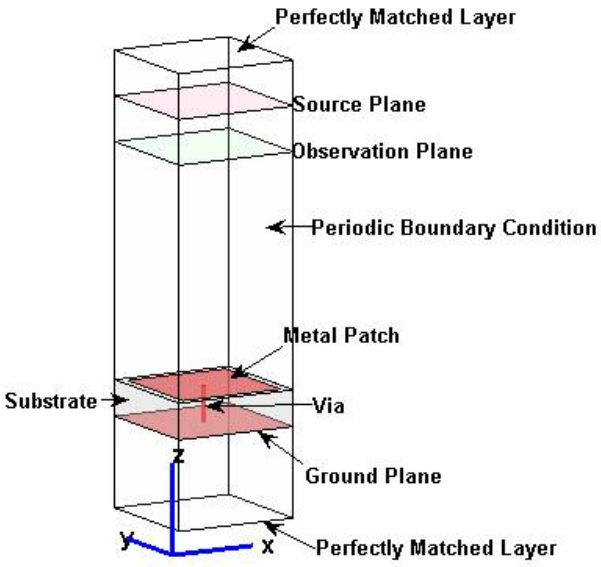

(a)

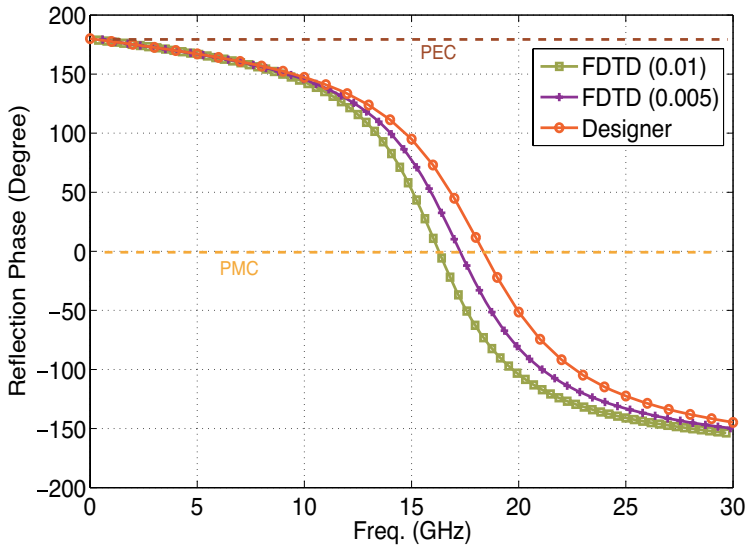

(b)

Figure 1. (a) FDTD simulation model of a mushroom-like EBG structure, and (b) reflection phase of the EBG structure with $0.01\lambda_{12\text{GHz}}$ and $0.005\lambda_{12\text{GHz}}$ grid sizes.

As observed in Fig. 1b, the reflection phase of the reference EBG changes continuously from 180° to −180°. Although the FDTD and Designer results show a noticeable frequency shift, they exhibit the same reflection phase pattern. The FDTD results approach the Designer results as the grid size becomes smaller. Due to the square geometry, there is no cross polarization. The resonant frequency is 17.2 GHz based on the FDTD simulation with $0.005\lambda_{12\text{GHz}}$ grid size and 18.2 GHz from the Ansoft Designer simulation.

2.2. Single Spiral AMC Design

The operation principle of the AMC surface can be simply explained by an equivalent LC circuit theory [14]. To increase the value of the equivalent inductor, a single spiral is placed on top of the grounded substrate to replace the square patch, as shown in Fig. 2a. The parameters of the substrate remain the same as the reference EBG in Fig. 1. The width of the spiral is $0.01\,\lambda_{12\text{GHz}}$. A y-polarized plane wave is normally incident on the AMC. Figure 2b shows the magnitudes of the reflection coefficients for both the co-polarized field and cross-polarized field. A large cross polarization can be found in the frequency band from 10 GHz to 30 GHz because of the asymmetric geometry. Four magnitude resonances can be found at 9.6 GHz, 13.1 GHz, 19.1 GHz, and 26.6 GHz. In Fig. 2c, the 0° phase exists at the same frequencies as the magnitude resonances. The first resonant frequency is 40.7% lower than the frequency observed by the metal patch of Fig. 1. Although it seems to meet the desired requirement in terms of surface compactness, the resulting high cross polarization is not acceptable in many applications.

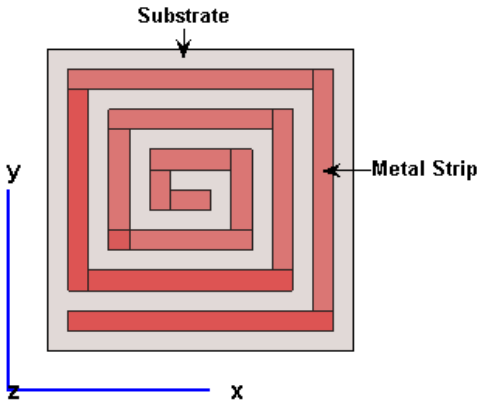

(a)

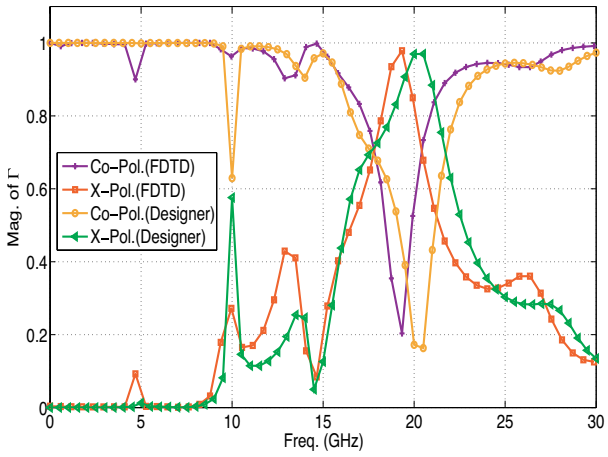

(b)

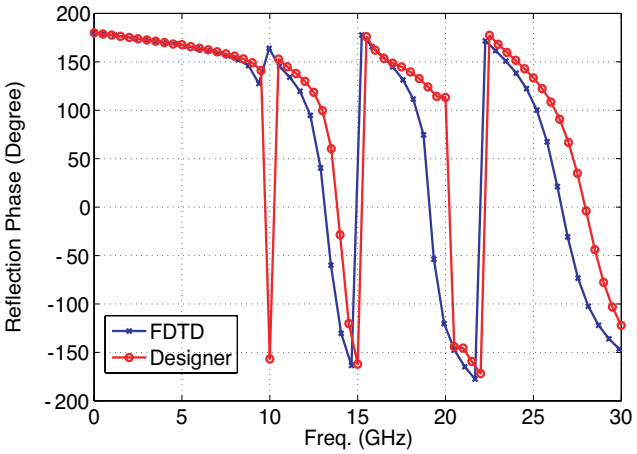

(c)

Figure 2. Single spiral geometry: (a) top view, (b) reflection magnitudes, and (c) reflection phases for the co-polarized fields.

2.3. Double Spiral AMC Design

Besides the single spiral case, two separate metal strip lines turning into the opposite direction are investigated, as shown in Fig. 3a. The width of spiral remains $0.01\,\lambda_{12\mathrm{GHz}}$. In Fig. 3b, a large cross polarization in the frequency range from 10 GHz to 30 GHz is observed. The double spiral generates two magnitude resonances at 10 GHz and 20.4 GHz, which correspond to the resonances of reflection phase as it can be

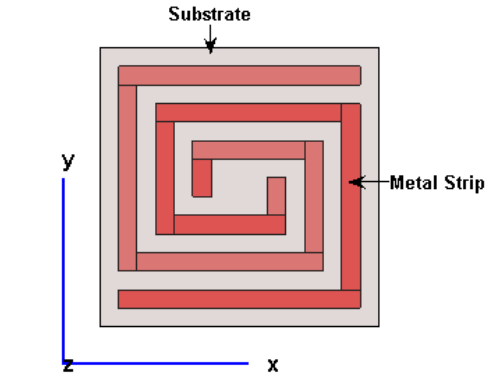

(a)

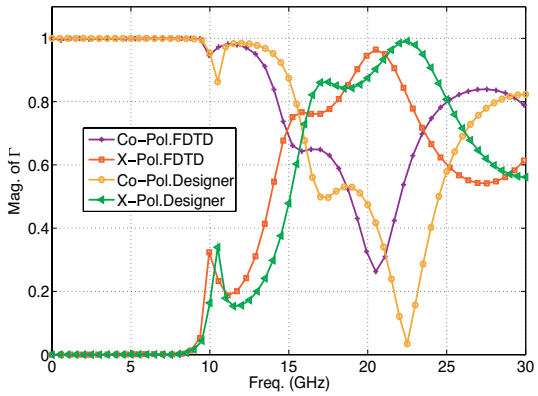

(b)

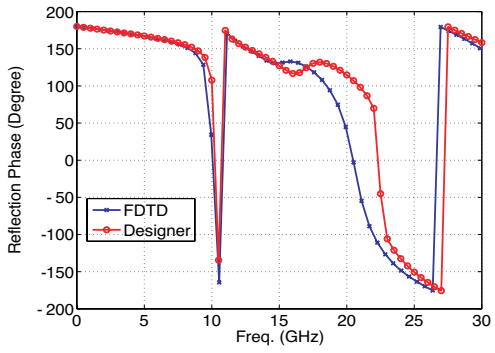

(c)

Figure 3. Double spiral geometry without center connection: (a) top view, (b) reflection magnitudes, and (c) reflection phases for the co-polarized fields.

seen in Fig. 3c.

To reduce the cross polarization, two separate spirals are connected by an additional metal strip line in the center, as shown in Fig. 4a. As a result of the center connection, the overall cross polarization has been reduced. The resonances of both reflection magnitude and phase can be found at 13.1 GHz and 27.4 GHz. From the simulated results, the magnitude of resonance, which exhibits severe cross polarization, matches to the phase resonance.

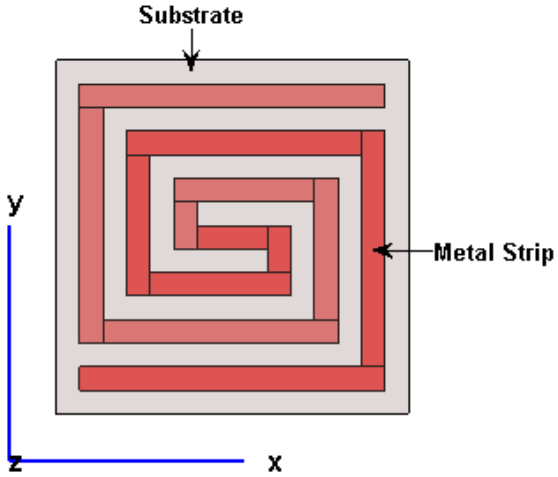

(a)

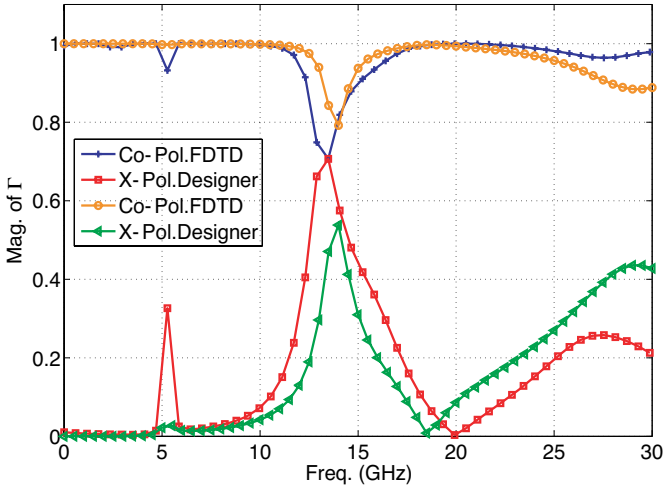

(b)

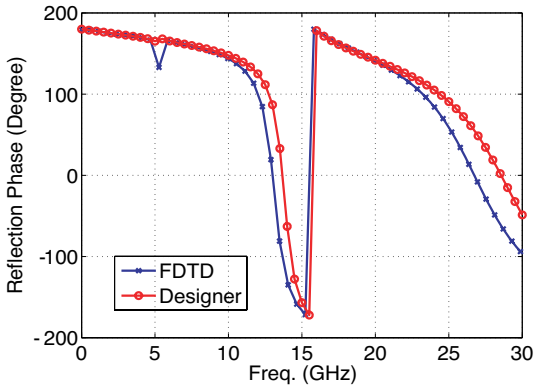

(c)

Figure 4. Double spiral geometry with center connection: (a) top view, (b) reflection magnitudes, and (c) reflection phases for the co-polarized fields.

In addition, the cross polarization affects the bandwidth of the reflection phase. In Figs. 3b and 3c, a sharp magnitude resonance at 10 GHz generates a narrow bandwidth of reflection resonance. On the other hand, the resonance at 20.4 GHz causes a relatively wide bandwidth of reflection phase. Usually, surface parameters such as substrate permittivity, substrate thickness, and gap width between periodic elements can change the operating frequency band and its bandwidth [6].

2.4. Four Arm Spiral AMC Design

Due to the significant cross polarization, the single and double spiral geometries are not good candidates for applications requiring low cross polarization. To eliminate the cross polarization, a four-arm spiral is explored, as shown in Fig. 5a. Four spiral branches, each with a $0.01\,\lambda_{12\mathrm{GHz}}$ width, split from the center and rotate outwards. In contrast to the previous designs, if this unit cell is rotated 90 degrees, it can exactly recover itself. Therefore, this symmetrical condition guarantees the same scattering response to the x- and y-polarized incident waves. As a result, no cross polarization is observed from this structure, as shown in Fig. 5b. In this case, the resonant frequency decreases as the number of spiral turns increase. The resonances of reflection phase can be found at 9.2 GHz and 21.2 GHz in Fig. 5c. In the Ansoft Designer data, a null in the co-polarized field is observed near 9.2 GHz, which may caused by an improper treatment of singularity

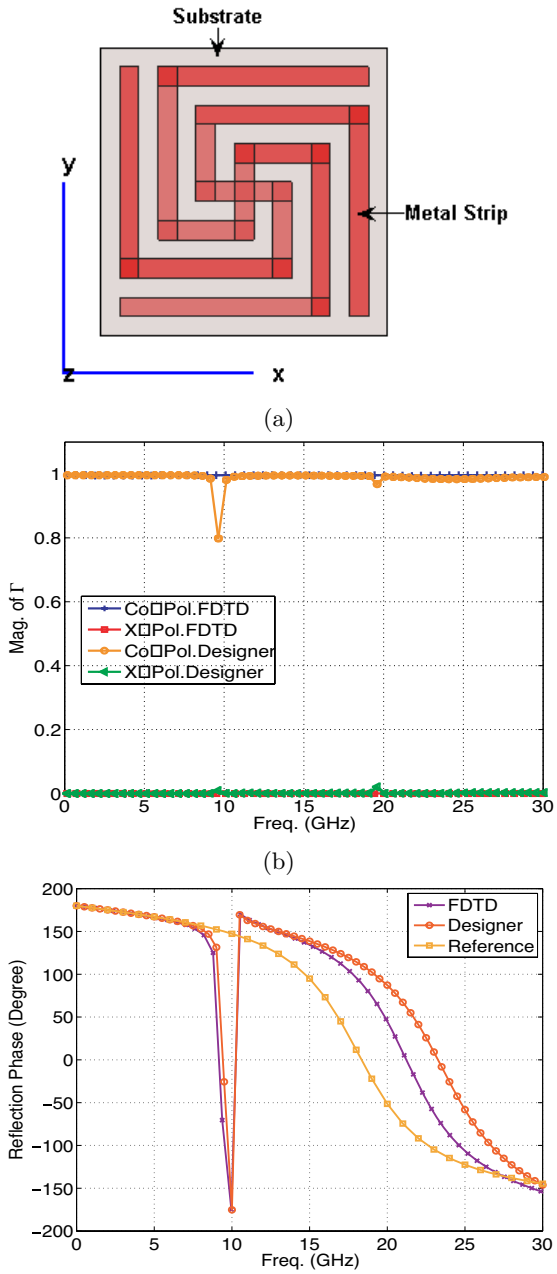

Figure 5. Four arm spiral geometry: (a) top view, (b) reflection magnitudes, and (c) reflection phases for the co-polarized fields.

near the resonance in MoM simulation. The first resonant frequency is 49.45% lower than the reference geometry in Fig. 1. Therefore, the compactness of a unit geometry is achieved without generating the cross polarization level. This significant reduction in size for a single element leads to a very attractive design feature for applications based on arrays composed of such an element.

3. CONCLUSIONS

Various configurations of printed spiral geometries have been examined to realize compact artificial magnetic conductor behavior in this paper. The compactness of electromagnetic band-gap surface can be achieved by increasing the equivalent inductance. However, it is revealed in this paper that both single and double spirals exhibit a large cross polarization level. Therefore, the four arm spiral geometry is proposed and designed to successfully eliminate the cross polarized fields. The proposed compact spiral AMC material is a good candidate for various antenna applications.

REFERENCES

1. Yang, R., Y. Xie, P. Wang, and L. Li, "Microstrip antennas with left-handed materials substrates," *J. of Electromagn. Waves and Appl.*, Vol. 20, No. 9, 1221–1233, 2006.
2. Grzegorczyk, T. M. and J. A. Kong, "Review of left-handed metamaterials: Evolution from theoretical and numerical studies to potential applications," *J. of Electromagn. Waves and Appl.*, Vol. 20, No. 14, 2053–2064, 2006.
3. Sui, Q., C. Li, L. L. Li, and F. Li, "Experimental study of $\lambda/4$ monopole antennas in a left-handed meta-material," *Progress In Electromagnetics Research*, PIER 51, 281–293, 2005.
4. Wu, B.-I., W. Wang, J. Pacheco, X. Chen, T. Grzegorczyk, and J. A. Kong, "A study of using metamaterials as antenna substrate to enhance gain," *Progress In Electromagnetics Research*, PIER 51, 295–328, 2005.
5. Yang, F., V. Demir, D. A. Elsherbeni, and A. Z. Elsherbeni, "Enhancement of printed dipole antennas characteristics using semi-EBG ground plane," *J. of Electromagn. Waves and Appl.*, Vol. 20, No. 8, 993–1006, 2006.
6. Yang, F. and Y. Rahmat-Samii, "Reflection phase characterizations of the EBG ground plane for low profile wire antenna ap-

plications," *IEEE Trans. Antennas Propag.*, Vol. 51, 2691–2703, Oct. 2003.

7. Nakano, H., K. Hitosugi, N. Tatsuzawa, D. Togashi, H. Mimaki, and J. Yamauchi, "Effects on the radiation characteristics of using a corrugated reflector with a helical antenna and an electromagnetic band-gap reflector with a spiral antenna," *IEEE Trans. Antennas Propagat.*, Vol. 53, No. 1, 191–199, Jan. 2005.
8. Abedin, M. F. and M. Ali, "Effects of EBG reflection phase profiles on the input impedance and bandwidth of ultra-thin directional dipoles," *IEEE Trans. Antennas Propagat.*, Vol. 53, No. 11, 3664–3672, Nov. 2005.
9. Yang, F. and Y. Rahmat-Samii, "Microstrip antennas integrated with electromagnetic band-gap (EBG) structures: a low mutual coupling design for array applications," *IEEE Transactions on Antennas and Propagation*, Vol. 51, No. 10, 2936–2946, October 2003.
10. Yang, L., M. Fan, and Z. Feng, "A spiral Electromagnetic Bandgap (EBG) structure and its application in microstrip antenna arrays," *APMC 2005 Proceedings*, Vol. 3, Dec. 2005.
11. Yao, Y., X. Wang, and Z. Feng, "A novel dual-band compact Electromagnetic Bandgap (EBG) structure and its application in multi-antennas," *IEEE Antennas Propag. Society International Symposium*, 1943–1946, July 2006.
12. Hosseini, M., A. Pirhadi, and M. Hakkak, "Design of a non-uniform high impedance surface for a low profile antenna," *J. of Electromagn. Waves and Appl.*, Vol. 20, No. 11, 1455–1464, 2006.
13. Poilasne, G., "Antennas on high-impedance ground planes: On the importance of the antenna isolation," *Progress In Electromagnetics Research*, PIER 41, 237–255, 2003.
14. Sievenpiper, D., L. Zhang, R. F. J. Broas, N. G. Alexopolus, and E. Yablonovitch, "High-impedance electromagnetic surfaces with a forbidden frequency band," *IEEE Trans. Microwave Theory Tech.*, Vol. 47, 2059–2074, Nov. 1999.
15. McVay, J. and N. Engheta, "High impedance metamaterial surfaces using Hilbert-curve inclusions," *IEEE Microwave and Wireless Components Letters*, Vol. 14, No. 3, 130–132, Mar. 2004.
16. Simovski, C. R., P. Maagt, and I. Melchakova, "High-impedance surfaces having stable resonance with respect to polarization and incidence angle," *IEEE Trans. Antennas and Propag.*, Vol. 53, No. 3, 908–914, Mar. 2005.
17. Hiranandani, M. A., A. B. Yakovlev, and A. A. Kishk, "Artificial

magnetic conductors realised by frequency-selective surfaces on a grounded dielectric slab for antenna applications," *IEE Proc. - Microw. Antennas Propag.*, Vol. 153, No. 5, 487–493, Oct. 2006.

18. Yang, F., J. Chen, Q. Rui, and A. Elsherbeni, "A simple and efficient FDTD/PBC algorithm for periodic structure analysis," *Radio Science*, Vol. 42, No. 4, RS4004, July 2007.